states, whereas the calculations refer to vertical energies based on the ground-state geometries. The calculations correctly account for the observed blue shift of the lowest energy singlet state of CrO_2F_2 relative to that of CrO_2Cl_2. A similar shift calculated for CrO_3X^- is not apparent in the experimental data.

Acknowledgment. This work was supported in part by a grant from the National Science Foundation.

Registry No. CrO_4^{2-}, 13907-45-4; CrO_3F^-, 17185-83-0; CrO_3Cl^-, 15906-70-4; CrO_2F_2, 7788-96-7; CrO_2Cl_2, 14977-61-8.

Contribution from the Department of Chemistry and Materials Science Center, Cornell University, Ithaca, New York 14853

Electronic Structure of One-Dimensional Linear Halogen-Bridged Gold Chains

Christoph Janiak and Roald Hoffmann*

Received January 27, 1989

The band structures of linear halogen-bridged mixed-valent gold chains of the form $\{Au^{III}X_2L_2\text{–}Au^{I}L_2\}_\infty$ (X = bridging Cl, Br; L = terminal-ligand SH_2, Cl, and/or H) were studied by using the extended Hückel method. The valence band was found to be a ligand lone-pair combination—a result unexpected from studies on analogous platinum chains. The variation of the band gap as a function of different geometries is in agreement with experimental results.

Introduction

Halogen-bridged one-dimensional metal complexes show interesting optical properties. Mixed-valence Pt^{II}/Pt^{IV} complexes containing $\cdots X\text{–}Pt^{IV}L_4\text{–}X\cdots Pt^{II}L_4\cdots$ linear chains (X = halogen, L = amine ligand) are the best known and extensively studied examples of these low-dimensional compounds.[1-3] Recent investigations on one-dimensional halogen-bridged complexes include X-ray structural studies[4-10] and Raman, resonance-Raman,[9-14] and electronic[9-18] spectroscopy. A perceptive theoretical analysis of the halogen-bridged platinum chains was carried out by Whangbo and Foshee.[19] A more general approach to linear M–X–M linkages in molecules, polymers, and extended networks was undertaken by Wheeler et al.[20]

Only a small number—albeit increasing—of halogen-bridged linear chains involving metals other than platinum, such as palladium,[3,6,8,13,15,21] nickel,[3,5,6,12,22] copper,[4] and gold are known. Compared to those of their platinum analogues, studies of the one-dimensional gold complexes, for instance $\{Au^{III}X_3(DBS)\text{–}Au^{I}X(DBS)\}_\infty$ (X = Cl, Br; DBS = dibenzyl sulfide, $S(CH_2C_6H_5)_2$), are scarce,[23-25] although their syntheses[26,27] and solid-state structure[23] were established quite early.

This paper is concerned with the differences and similarities in the electronic structures of the one-dimensional Au and Pt complexes.[19] Our work was stimulated by a recent paper by Tanino et al.[25]

Results and Discussion

According to a recent single-crystal X-ray structural investigation, $AuCl_2(DBS)$ consists of alternating $Au^{III}Cl_3(DBS)$ and $Au^{I}Cl(DBS)$ units in a neutral, almost linear chain, shown schematically in **1**.[25,28]

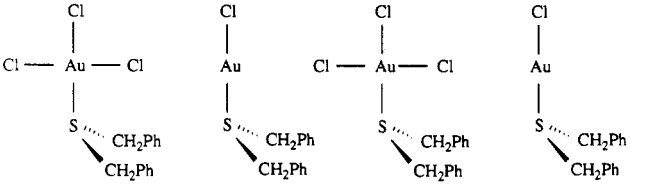

1

Different chains slip in random fashion, owing to a weak three-dimensional correlation (disorder perpendicular to the chains), to give two statistically half-occupied halide positions: Thus, the bridging chlorines appear disordered in the crystal

(1) Day, P. In *Low-Dimensional Cooperative Phenomena*; Keller, H. J., Ed.; Plenum Press: New York, 1975; p 191.
(2) Keller, H. J. In *Extended Linear Chain Compounds*; Miller, J. S., Ed.; Plenum Press: New York, 1982; Vol. 1, p 357.
(3) Clark, R. J. H. In *Advances in Infrared and Raman Spectroscopy*; Clark, R. J. H., Hester, R. E., Eds.; Wiley: New York, 1984; Vol. 11, p 95.
(4) Oshio, H.; Toriumi, K.; Bando, S. *Chem. Lett.* **1988**, 1713.
(5) Evans, J.; Gauntlett, J. T.; Levason, W. *Inorg. Chem.* **1988**, *27*, 4521.
(6) Toriumi, K.; Yamashita, M.; Murase, I. *Chem. Lett.* **1986**, 1753.
(7) Tanaka, M.; Tsujikawa, I.; Toriumi, K.; Ito, T. *Acta Crystallogr.* **1986**, *C42*, 1105.
(8) Toriumi, K.; Yamashita, M.; Ito, H.; Ito, T. *Acta Crystallogr.* **1986**, *C42*, 963.
(9) Fanizzi, F. P.; Natile, G.; Lanfranchi, M.; Tiripicchio, A.; Clark, R. J. H.; Kurmoo, M. *J. Chem. Soc., Dalton Trans.* **1986**, 273.
(10) Clark, R. J. H.; Croud, V. B.; Dawes, H. M.; Hursthouse, M. B. *J. Chem. Soc., Dalton Trans.* **1986**, 403.
(11) Clark, R. J. H.; Croud, V. B.; Khokhar, A. R. *Inorg. Chem.* **1987**, *26*, 3284.
(12) Clark, R. J. H.; Croud, V. B. *Inorg. Chem.* **1986**, *25*, 1751.
(13) Clark, R. J. H.; Croud, V. B.; Kurmoo, M. *J. Chem. Soc., Dalton Trans.* **1985**, 815.
(14) Clark, R. J. H.; Kurmoo, M. *J. Chem. Soc., Dalton Trans.* **1985**, 579.
(15) Wada, Y.; Mitani, T.; Yamashita, M.; Koda, T. *J. Phys. Soc. Jpn.* **1985**, *54*, 3143.
(16) Tanaka, M.; Kurita, S.; Fujisawa, M.; Matsumoto, S. *J. Phys. Soc. Jpn.* **1985**, *54*, 3632.
(17) Wada, Y.; Mitani, T.; Yamashita, M.; Koda, T. *Synth. Met.* **1987**, *19*, 907.
(18) Tanaka, M.; Kaneko, W.; Kurita, S.; Yamada, A.; Fukutani, H. *J. Phys. Soc. Jpn.* **1987**, *56*, 1197.
(19) Whangbo, M.-H.; Foshee, M. J. *Inorg. Chem.* **1981**, *20*, 113.
(20) Wheeler, R. A.; Whangbo, M.-H.; Hughbanks, T.; Hoffmann, R.; Burdett, J. K.; Albright, T. A. *J. Am. Chem. Soc.* **1986**, *108*, 2222. See also: Burdett, J. K. *Inorg. Chem.* **1978**, *17*, 2537. Lauher, J. W. *Inorg. Chem.* **1980**, *39*, 119. Burdett, J. K. *Comments Inorg. Chem.* **1981**, *1*, 85.
(21) Clark, R. J. H.; Croud, V. B.; Kurmoo, M. *Inorg. Chem.* **1984**, *23*, 2499.
(22) Cooper, D. A.; Higgins, S. J.; Levason, W. *J. Chem. Soc., Dalton Trans.* **1983**, 2131.
(23) Brain, F. H.; Gibson, C. S.; Jarvis, J. A. J.; Phillips, R. F.; Powell, H. M.; Tyabji, A. *J. Chem. Soc.* **1952**, 3686.
(24) Interrante, L. V.; Bundy, F. P. *J. Inorg. Nucl. Chem.* **1977**, *39*, 1333.
(25) Tanino, H.; Takahashi, K.; Tajima, M.; Kato, M.; Yao, T. *Phys. Rev.* **1988**, *B38*, 8327.
(26) Herrmann, F. *Ber. Dtsch. Chem. Ges.* **1905**, *38*, 2813.
(27) Smith, G. M. *J. Am. Chem. Soc.* **1922**, *44*, 1769.
(28) Takahashi, K.; Tanino, H. *Chem. Lett.* **1988**, 641.

0020-1669/89/1328-2743$01.50/0

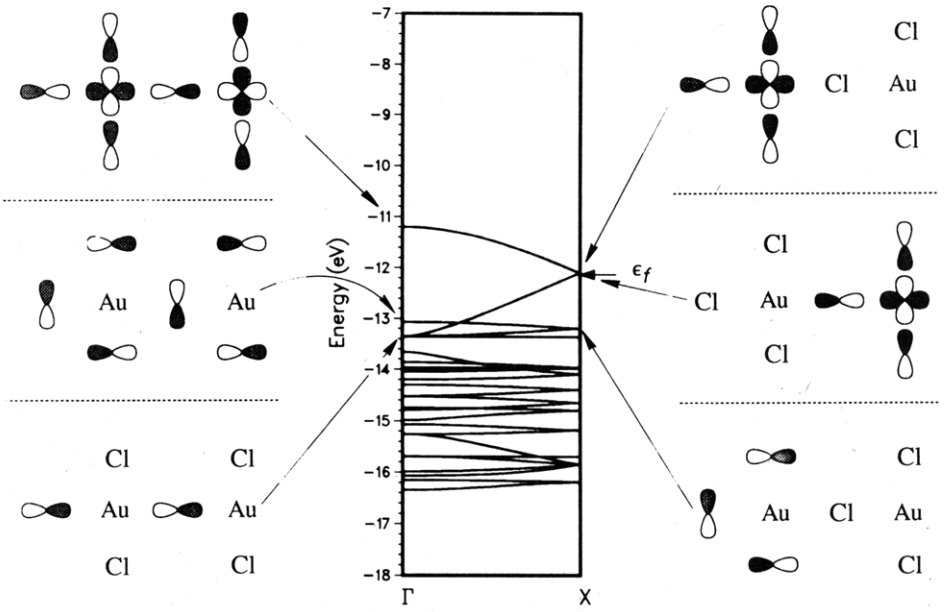

Figure 1. Band-structure diagram for the $\{Au^{II}Cl_3-Au^{II}Cl_3\}_\infty^{2-}$ chain. The orbital representations are schematic, and only features that will be of importance for the distorted chain are shown.

structure.[2,29] An additional feature of the crystal structure is the pairing of two one-dimensional chains at an interchain distance of 332 pm.[25,28] However, according to our band-structure calculation this interaction is too weak to effect the valence or conduction band, leading merely to a simple doubling of these bands. Therefore, we considered only single chains in our following calculations. For simplicity, we decided to replace the bulky dibenzyl sulfide ligand by SH_2 (**1** → **2**). Further studies with Cl^- (**2** → **3**) and H^- (**2** → **4**) as model ligands helped us to understand the sulfur case.

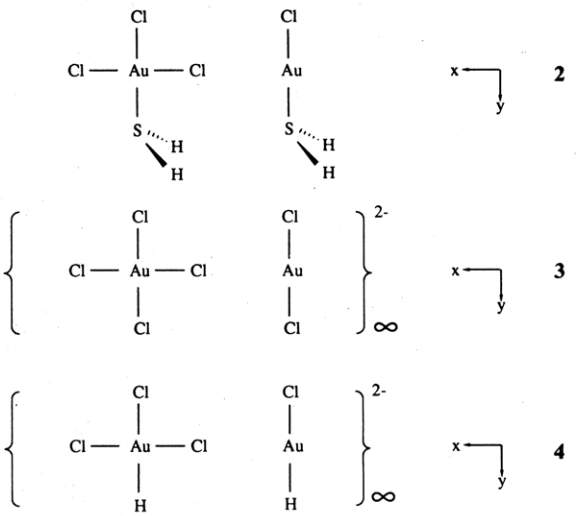

It is helpful to start this theoretical study by regarding **2**–**4** as distorted geometries of an ideal symmetric chain of $Au^{II}Cl_2L$ units, as shown in **5** (L = SH_2 (**a**), Cl^- (**b**), H^- (**c**)).

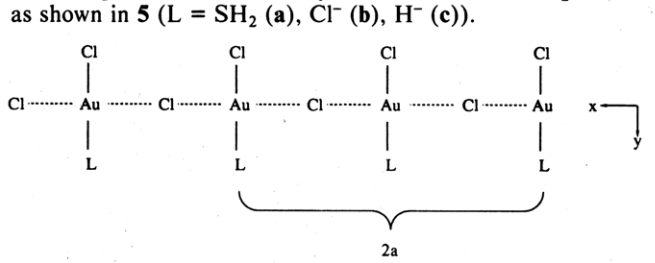

5a–c

In **5** the bridging chlorine is located at the midpoint of the distance between the two golds. Model chains **3** and **4** and their undistorted forms **5b** and **5c** display great similarities in their band structure, so in the following we just refer to **3** and **5b**.

Figure 1 shows a piece of the band-structure diagram for **5b**, with the assignment of the bands around the Fermi level, which are made up primarily of antibonding combinations of Au $d_{x^2-y^2}$, the bridging Cl p_x, and terminal Cl p_y orbitals. In addition, one more relevant band is assigned in Figure 1, namely the antibonding combination between the bridging Cl p_y and terminal Cl p_x orbitals, placed at about −13.1 eV. The reason for singling out this ligand lone-pair band will become apparent. Two unit cells were chosen as the repeat distance (=2*a*), hence all bands are folded; i.e., degeneracies are induced at the zone edge ($k = \pi/2a$).

The symmetric, undistorted combination of d^9 Au^{II} species leads to a half-filled band, as seen in Figure 1. In its low-spin arrangement structure **5b** represents a one-dimensional metal, which according to the Peierls theorem[30]—the solid-state analogue of the Jahn–Teller theorem—will be subject to distortion so as to create an energy gap at the Fermi level. The degeneracies at $k = \pi/2a$ in Figure 1, induced by choosing a doubled unit cell, can be lifted easily by a geometrical distortion that really does double the unit cell size.[31] The observed distortion to give structure **3** is a "dimerization of the bridging chlorine subchain", creating a Au^{III}–Au^{I} alternation by moving two bridging ligands closer to each second Au^{II}. This can be classified as a first-order (i.e. degeneracy lifting at the Fermi level), and likely low-spin ($2k_f$), Peierls distortion.[31]

The resulting band-structure diagram for structure **3** is shown in Figure 2. Two additional band diagrams for chains with a Au–Cl distance intermediate between those of **5b** and **3** allow us to visualize easier the changes in the valence and conduction band. From the orbital picture in Figure 1 it is easy to rationalize the rise in energy of the conduction band upon distortion. This is due to an increased antibonding overlap between Au^{III} $d_{x^2-y^2}$ and bridging Cl p_x. The valence band is lowered in energy, except in the vicinity of $k = 0$ where it remains essentially unchanged—as anticipated from the orbital picture. However, the valence band in Figure 1 (structure **5b**) does not become the new valence band in Figure 2 (structure **3**). Upon distortion, the antibonding all-

(29) Keller, H. J.; Keppler, B.; Ledezma-Sanchez, G.; Steiger, W. *Acta Crystallogr.* **1981**, *B37*, 674.

(30) Peierls, R. E. *Quantum Theory of Solids*; Oxford Univ. Press: London, 1975; p 108.

(31) Whangbo, M.-H. In *Crystal Chemistry and Properties of Materials with Quasi-One-Dimensional Structures*; Rouxel, J., Ed.; D. Reidel: Dordrecht, The Netherlands, 1986; p 27.

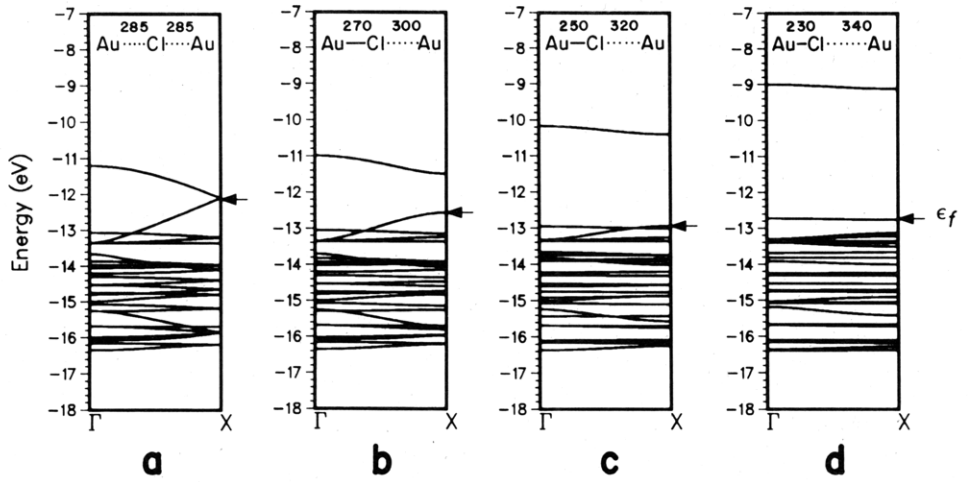

Figure 2. Changes in the band-structure diagram on going from a symmetrical chain (**5b**) to a localized one (**3**): (a) Au^{II}–Cl = 285 pm, d = 0 pm (d = displacement of bridging chlorine from the midpoint between the two golds; see **8**); (b) Au^{III}–Cl = 270 pm, d = 15 pm; (c) Au^{III}–Cl = 250 pm, d = 35 pm; (d) Au^{III}–Cl = 230 pm, d = 55 pm.

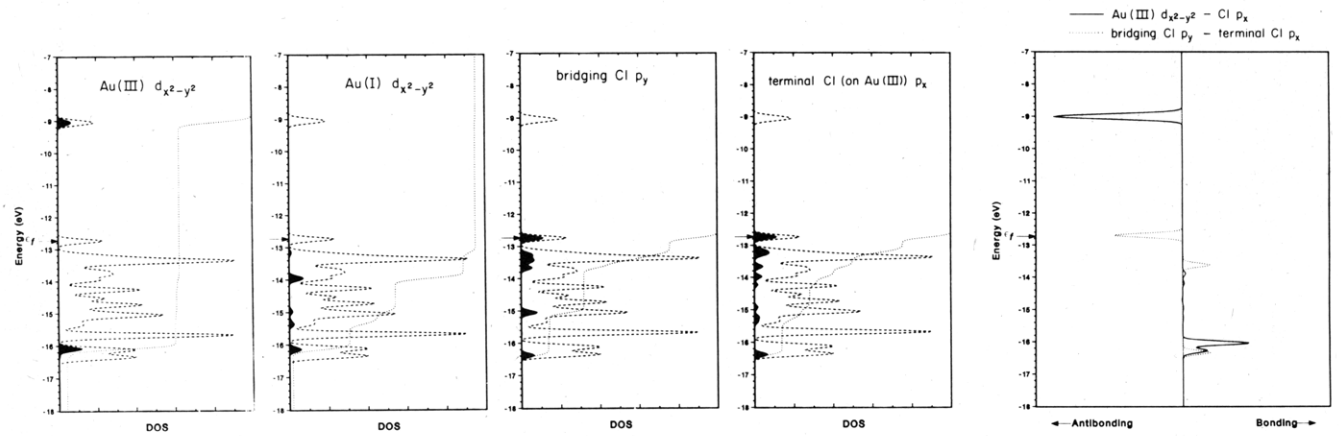

Figure 3. First four panels: Density-of-state (DOS) plots for selected orbitals in **3** (shaded area) with integration (dotted line) and total DOS (dashed line). Right-hand panel: Projected overlap population between the bridging Cl p_y and terminal Cl p_x orbitals (average −0.013, dotted line) and between the Au^{III} $d_{x^2-y^2}$ and bridging Cl p_x orbitals (average 0.090, solid line) in **3**.

filled orbital combination of the chlorine p-type "lone pairs" shown in Figure 1 is raised in energy by about 0.4 eV to become the valence band in **3**, while the Au^{I} $d_{x^2-y^2}$ orbital combinations fall below the Fermi level. This may be seen from the density-of-state plot and its decomposition into contributions from various atoms (Figure 3). The conduction band in **3** is solely an antibonding combination of the Au^{III} $d_{x^2-y^2}$, bridging Cl p_x, and terminal $Cl(Au^{III})$ p_y orbitals (see right-hand panel in Figure 3).

This finding reveals a substantial difference from the $\{Pt^{IV}(NH_3)_4Cl_2–Pt^{II}(NH_3)_4\}_\infty^{4+}$ chain. There, the Pt^{II} d_{z^2} orbital becomes part of the valence band, while the Pt^{IV} d_{z^2} orbital forms the conduction band.[19] Initially, it was thought that the electronic structure and spectroscopy of the d^8–d^{10} gold chains resemble closely those of the d^6–d^8 platinum complexes. In the halogen-bridged mixed-valence platinum systems the lowest energy visible absorption band is assigned as a metal to metal charge-transfer intervalence transition from the occupied d_{z^2} Pt^{II} (valence band) to the unoccupied d_{z^2} Pt^{IV} (conduction band). Considering the different coordination geometry for the gold complexes (quasi square planar vs quasi-octahedral for Pt), the charge-transfer transition was subsequently assigned to arise from $d_{x^2-y^2}$ Au^{I} to $d_{x^2-y^2}$ Au^{III}.[24,25] However, in light of our calculation the model gold chain **3** would have a ligand to metal excitation as its lowest energy transition. The origin for this difference between the gold and platinum chains lies (a) in the higher energy Pt 5d orbitals relative to Au 5d and (b) in the absence of "lone-pair" orbitals on the nitrogen of the NH_3 donor ligand (other than the lone pair used in dative bonding to the metal) in the platinum chain, eliminating high-energy filled ligand-orbital combinations. Figure 4 shows the relative energy ordering of the metal d and ligand

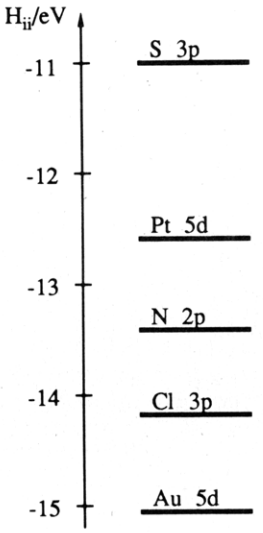

Figure 4. Selected orbital energies.

atom p orbitals under consideration.

The flat bands in Figure 2 indicate strongly localized electronic states, as was also found in the distorted platinum chain.

Now, we will return almost to the starting point of our discussion, to the SH_2-ligated alternating $\{Au^{III}Cl_3(SH_2)–Au^{I}Cl(SH_2)\}_\infty$ chain **2**. The band structure diagram for **2** is given in Figure 5. Comparing Figures 5 and 2d, one notes two additional bands right at the (raised) Fermi level. The origin of these bands

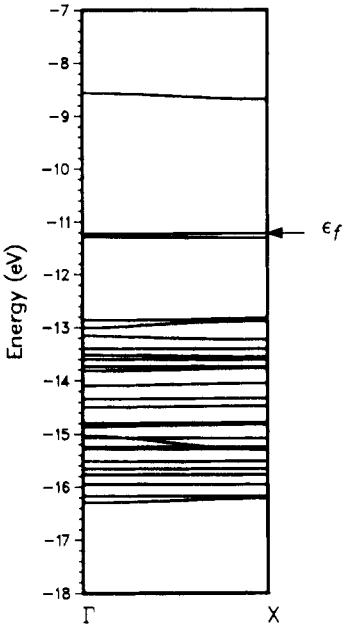

Figure 5. Band-structure diagram (excerpt) for the $\{Au^{III}Cl_3(SH_2)$–$Au^{I}Cl(SH_2)\}_\infty$ chain, **2**.

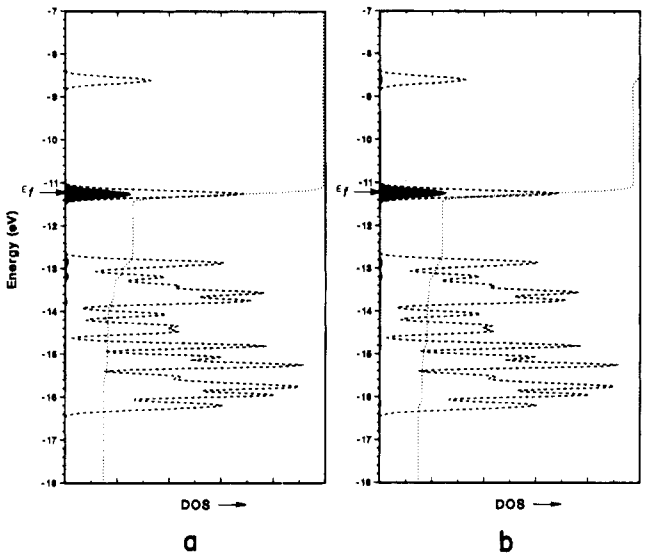

Figure 6. Density-of-state (DOS) plots for the sp^3-approximated lone-pair orbital on sulfur, bonded to Au^{I} (a) and Au^{III} (b) in **2** with integration of the projected DOS (dotted line) and total DOS (dashed line).

is clear—the sulfur in SH_2, even when bonded as a ligand, still has a nonbonding pair of electrons. The S lone pair is pointed away from the chain direction and along the pseudo-3-fold axis of the $SAuCl_2$ pyramid. The lone pair thus avoids interaction with the bridging Cl p_y lone-pair orbitals. In a first approximation the S lone pair can be regarded as an sp^3-hybrid orbital. Assuming a perfect tetrahedral geometry around sulfur and in the Cartesian coordinate system shown for **2**, an idealized hybrid lone-pair orbital would have the form $\Phi = {}^1/_2s + 2/\sqrt{6}p_x - 1/\sqrt{12}p_y$.[32] Figure 6 shows the contribution to the total density of state of such a combination for each of the two slightly different S atoms. The lone-pair valence band assignment is clearly confirmed. The dispersion of the lone-pair bands below −18 eV is due to the overestimation of a sulfur s-orbital participation ($H_{3s}(S) = -20.0$ eV) in the lone-pair hybrid by our simple approximation. Separate DOS plots for the sulfur p_x and p_y orbitals show the nonbonding electron pair to be mainly a p_x–p_y combination, with p_x being the major component. The nature of the conduction band does not change upon going from **3** to **2**.

(32) Cotton, F. A. *Chemical Applications of Group Theory*, 2nd ed.; Wiley-Interscience: New York, 1971; Chapter 8.5, p 213.

Table I. Comparison of Band (Orbital) Gaps to Absorption Energies in Gold Complexes

compd	theoretical gap[a]/eV	abs energy[b]/eV
$Au^{III}Cl_3(DBS)$[c]	2.60	>2.60
$\{Au^{III}Cl_3(DBS)$–$Au^{I}Cl(DBS)\}_\infty$ (**1**, **2**)	2.53	2.24
$Au^{III}Br_3(DBS)$[d]	2.14	~2.04
$\{Au^{III}Br_2Cl(DBS)$–$Au^{I}Cl(DBS)\}_\infty$ (**6**)	2.11	1.90
$\{Au^{III}Br_3(DBS)$–$Au^{I}Br(DBS)\}_\infty$ (**7**)	1.99	1.87

[a] DBS (=dibenzyl sulfide) substituted by SH_2 for the theoretical calculation. [b] Threshold energy of absorption spectra with α = 500 cm^{-1}, **E**||**x**; see ref 25. [c] $d(Au^{III}$–Cl) = 230 pm. [d] $d(Au^{III}$–Br) = 242 pm.

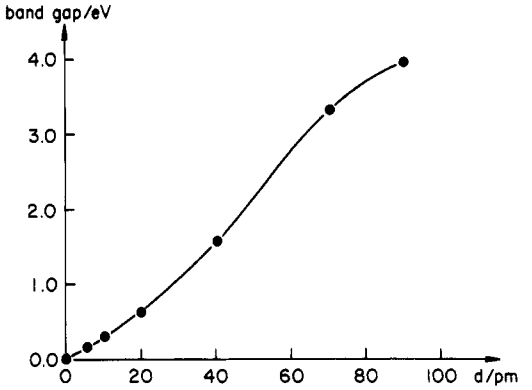

Figure 7. Band gap in the $\{Au^{III}Cl_3(SH_2)$–$Au^{I}Cl(SH_2)\}_\infty$ chain, **2**, as a function of *d*.

The effect of the ligands on the character of the valence band, and consequently the electronic transition, in the gold chains becomes even more obvious in **2**. Hence, an experimental approach to optimize desirable properties of the gold chains should consist in altering and tuning the terminal Au ligands so as to adjust the band gap.

Interpretation of Other Experimental Results.[24,25] The energy shifts observed in the electronic absorption spectra upon substituting chlorine by bromine in **1** can be reproduced by our band-structure calculation. We took structures **6** and **7** as model compounds.

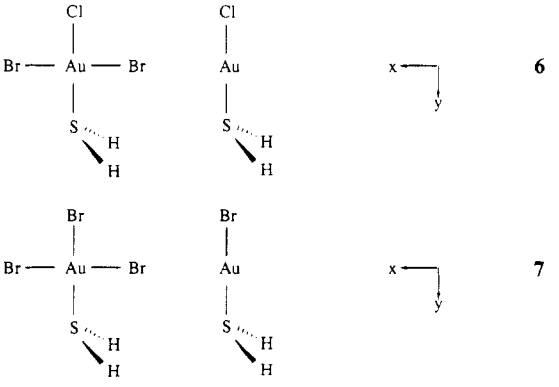

Table I compares the calculated band gaps for **2**, **6**, and **7** with experimental values for the respective dibenzyl sulfide ligated derivatives. Also included in Table I are HOMO–LUMO gaps for the monomeric species $Au^{III}X_3(SH_2)$ (X = Cl, Br). The decrease in the band gap by substituting the bridging chlorine for bromine (**2** → **6**) is not due to a change in elemental properties. Thus, keeping the Au–X distance the same for Cl and Br actually increases the band gap slightly for the latter. The decrease in band gap is due to the fact that the bromine is more centrally placed compared to chlorine. This is a consequence of the longer Au^{III}–Br bond length, while the $Au^{I}\cdots X$ separation remains relatively insensitive to changes in X, thus keeping the $Au^{III}\cdots Au^{I}$ distance constant.[25] Other things being equal, the band gap varies

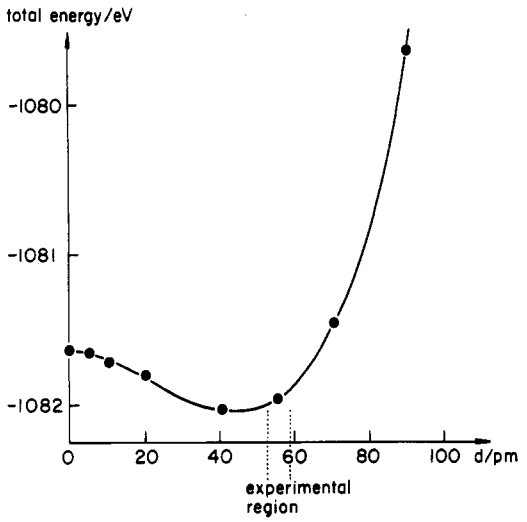

Figure 8. Total energy per $\{Au^{III}Cl_3(SH_2)-Au^{I}Cl(SH_2)\}$ unit in **2** as a function of d.

strongly with the displacement of the bridging halogenide from the midpoint d (see **8**) or the Au^{III}–X and $Au^{I}\cdots$X bond lengths,

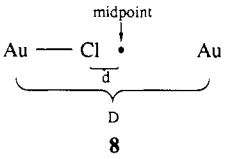

8

respectively, as was demonstrated qualitatively in Figure 2 and as is illustrated more quantitatively in Figure 7. This agrees well with general observations for the platinum chains.[3,16]

The charge-transfer exciton transition into a conduction band formed by antibonding Au^{III}–ligand orbital combinations also explains the large Stokes shift to lower energy for the corresponding luminescense. Populating this antibonding crystal orbital will lengthen the Au^{III}–ligand bonds. Consequently, the decreased band gap can be accounted for by a lower crystal field splitting of the Au^{III} 5d orbitals or a more central placing of the bridging halide. Both effects operate in the same direction.

Plotting the total energy per unit cell versus the halide displacement d (see **8**) in Figure 8 gives a local minimum close to the experimentally observed value.

The band-structure calculation could also explain the increase in conductivity under pressure and its anomalous decrease at very high pressure.[24] Lowering the Au^{III}–Au^{I} separation D (see **8**) to simulate a pressure effect—while other bond lengths are kept equal—decreases the band gap as the halide becomes more centrally placed (Figure 9). On the other hand, bringing the terminal SH_2 and X ligand closer to the Au^{III} atom increases the crystal field splitting and thus the band gap (Figure 10). The initial increase in the (still thermally activated) conductivity can be assumed being due to the decrease in the "soft" Au^{III}–Au^{I} separation. Eventually the metal–metal separation will saturate, and a turnover in conductivity at very high pressure would correspond to the increase in crystal field splitting—caused by the terminal ligand–metal bond decrease—becoming more dominant. The bromide complex also gives the more conductive complex (as was found experimentally), for reasons explained above.

Conclusions

In linear gold chains of the general formula $\{Au^{III}X_2L_2-Au^{I}L_2\}_\infty$ (X = bridging halogen, L = terminal ligands with an additional lone pair) the valence band most likely consists of a ligand lone-pair combination, with a possible participation of the bridging-halogen lone pair. The conduction band is an antibonding Au^{III} $d_{x^2-y^2}$ ligand σ-orbital combination. Therefore, the lowest energy absorption should be described as a ligand-to-metal charge-transfer excitation and not as an intervalence transition.

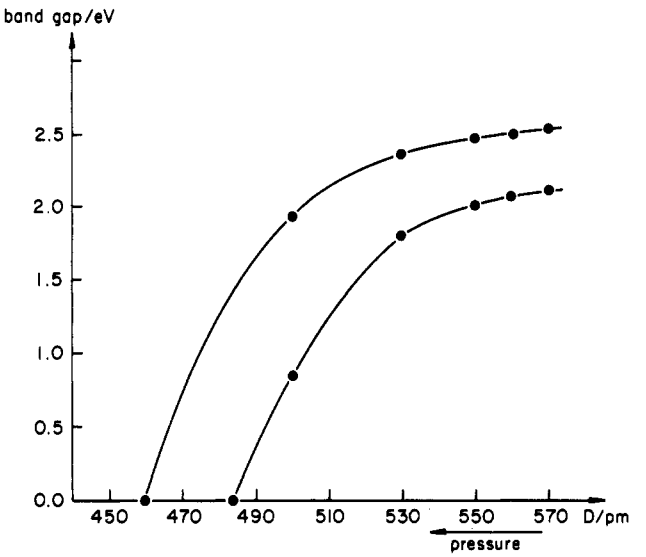

Figure 9. Band gaps in **2** (upper curve) and **6** (lower curve) as a function of D.

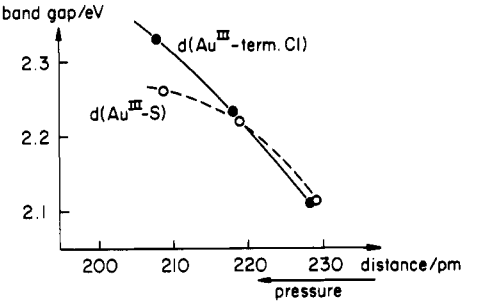

Figure 10. Band gap in **6** as a function of the Au^{III}–terminal Cl and Au^{III}–S bond lengths.

Appendix

The computations were carried out by using a tight-binding scheme[33] based upon the extended Hückel method.[34] Parameters were taken from previous work (H_{ii}, Slater exponents) as follows. Au[35]: 6s, −10.92 eV, 2.60; 6p, −5.55 eV, 2.58; 5d, −15.07 eV, 6.16 (0.6851) and 2.79 (0.5696) (a double-ζ expansion was used with the expansion coefficients given in parentheses). Cl[36]: 3s, −26.3 eV, 2.18; 3p, −14.2 eV, 1.73. Br[37]: 4s, −22.07 eV, 2.59; 4p, −13.10 eV, 2.13. H[34a]: 1s, −13.6 eV, 1.3. S[38]: 3s, −20.0 eV, 2.12; 3p, −11.0 eV, 1.83. A 25-k-point set was used for the properties to be averaged over the Brillouin zone.

The basic geometries for the model compounds in our calculation were taken from ref 25 and 28. If not stated otherwise, the bond lengths were fixed as follows: Au^{III}–Au^{I} = 570 pm, Au–terminal Cl = 228 pm, Au–S = 229 pm, Au–H = 150 pm, S–H = 134 pm ($\angle$AuSH = 109.5°), Au–terminal Br = 242 pm, Au^{III}–bridging Cl = 230 pm, $Au^{I}\cdots$bridging Cl = 340 pm, Au^{II}–bridging Cl = 285 pm. A linear- and planar-chain geometry was employed with 90° angles between the ligands.

Acknowledgment. This work was supported by a fellowship for C.J. from the scientific committee of NATO via the DAAD and by Research Grant CHE 8406119 from the National Science Foundation.

(33) Whangbo, M.-H.; Hoffmann, R.; Woodward, R. B. *Proc. R. Soc. London, Ser. A* **1979**, *A366*, 23.
(34) (a) Hoffmann, R. *J. Chem. Phys.* **1963**, *39*, 1397. (b) Hoffmann, R.; Lipscomb, W. N. *Ibid.* **1962**, *36*, 2179.
(35) Komiya, S.; Albright, T. A.; Hoffmann, R.; Kochi, J. K. *J. Am. Chem. Soc.* **1977**, *99*, 8440.
(36) Summerville, R. H.; Hoffmann, R. *J. Am. Chem. Soc.* **1976**, *98*, 7240.
(37) Hinze, J.; Jaffé, H. H. *J. Phys. Chem.* **1963**, *67*, 1501.
(38) Chen, M. M. L.; Hoffmann, R. *J. Am. Chem. Soc.* **1976**, *98*, 1647.